Article

Cell Systems

Emergent Gene Expression Responses to Drug Combinations Predict Higher-Order Drug Interactions

Graphical Abstract

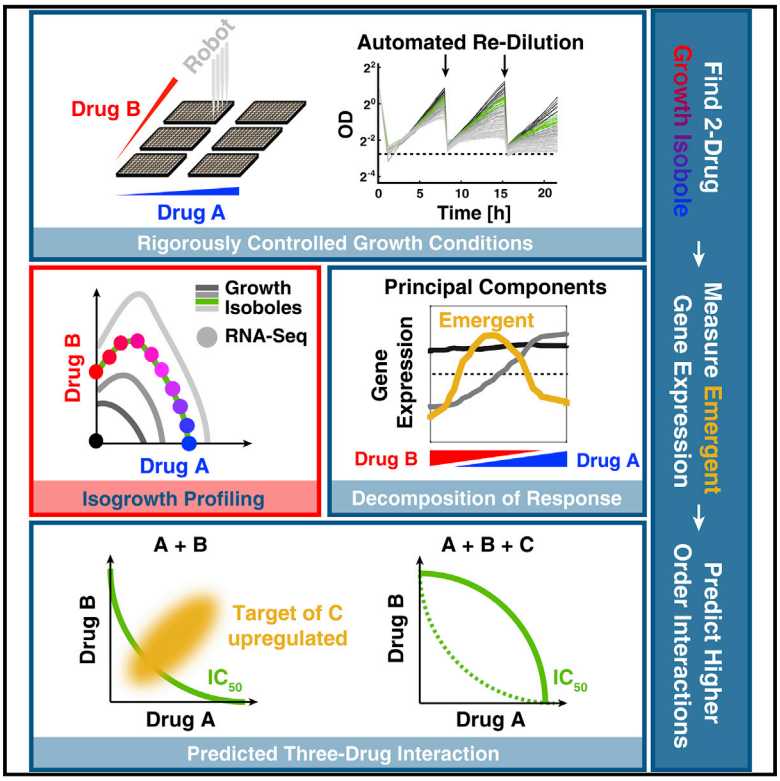

Highlights

- Rigorous control of growth rate is key to understanding response to drug combinations
- Three readily interpretable principal components (PCs) explain >90% of variance
- The 2nd PC exposes responses to individual drugs, revealing a new effect of myriocin
- The 3rd PC captures emergent responses and can predict antagonism with a third drug

Authors

Martin Lukačišin, Tobias Bollenbach

Correspondence

t.bollenbach@uni-koeln.de

In Brief

Effective design of combination therapies requires understanding the changes in cell physiology resulting from drug interactions. We show that the genome-wide transcriptional response of *S. cerevisiae* to combinations of two drugs can expose specific individual drug effects and predict higher-order antagonism with a third drug. Disentangling the global transcriptional response required a new approach for rigorously controlling growth rate. We provide a readily applicable recipe for uncovering emergent responses in other systems and for combinations of larger numbers of drugs.

Lukačišin & Bollenbach, 2020, Cell Systems *10*, 1–11
January 22, 2020
https://doi.org/10.1016/j.cels.2019.10.004

CellPress

Please cite this article in press as: Lukačišin and Bollenbach, Emergent Gene Expression Responses to Drug Combinations Predict Higher-Order Drug Interactions, Cell Systems (2019), https://doi.org/10.1016/j.cels.2019.10.004

Cell Systems
Article

Emergent Gene Expression Responses to Drug Combinations Predict Higher-Order Drug Interactions

Martin Lukačišin[1,2,3] and Tobias Bollenbach[1,4,*]
[1]Institute for Biological Physics, University of Cologne, 50937 Cologne, Germany
[2]IST Austria, 3400 Klosterneuburg, Austria
[3]Present address: Faculty of Medicine, Technion-Israel Institute of Technology, Haifa 32000, Israel
[4]Lead Contact
*Correspondence: t.bollenbach@uni-koeln.de
https://doi.org/10.1016/j.cels.2019.10.004

SUMMARY

Effective design of combination therapies requires understanding the changes in cell physiology that result from drug interactions. Here, we show that the genome-wide transcriptional response to combinations of two drugs, measured at a rigorously controlled growth rate, can predict higher-order antagonism with a third drug in *Saccharomyces cerevisiae*. Using isogrowth profiling, over 90% of the variation in cellular response can be decomposed into three principal components (PCs) that have clear biological interpretations. We demonstrate that the third PC captures emergent transcriptional programs that are dependent on both drugs and can predict antagonism with a third drug targeting the emergent pathway. We further show that emergent gene expression patterns are most pronounced at a drug ratio where the drug interaction is strongest, providing a guideline for future measurements. Our results provide a readily applicable recipe for uncovering emergent responses in other systems and for higher-order drug combinations. A record of this paper's transparent peer review process is included in the Supplemental Information.

INTRODUCTION

Combinatorial drug treatment is an increasingly important strategy for combating microbial infections and a powerful tool for understanding the molecular biology of the perturbed cell (Chen and Lahav, 2016; Fischbach, 2011; Pemovska et al., 2018). When two or more drugs are combined, synergistic or antagonistic interactions can occur. These interactions, respectively, correspond to increased or decreased inhibitory effect of the drug combination compared to the null expectation of additivity (Figure 1A; Bollenbach, 2015; Loewe, 1928). In recent years, high-throughput techniques for identifying drug interactions (Brochado et al., 2018; Cokol et al., 2011, 2014) and their modifiers (Chevereau and Bollenbach, 2015) have considerably advanced our understanding of drug interactions. Further, frameworks for quantifying higher-order drug interactions have been developed (Cokol et al., 2017; Russ and Kishony, 2018; Tekin et al., 2016). However, to rationally design combination therapies, a deeper understanding of the combinatorial effects of drugs on cell physiology and of the general principles guiding the cellular response to drug combinations is necessary (Cohen et al., 2008).

Predicting cellular responses to combinatorial perturbations from responses to the individual perturbations is one of the key conceptual goals of systems biology (Molinelli et al., 2013). In *Escherichia coli*, gene expression responses to combinations of two antibiotics, measured using fluorescent reporters for ~100 genes, can be predicted by a linear or nonlinear interpolation of the responses to the individual drugs (Bollenbach and Kishony, 2011). Another study showed that even the temporal response of ~100 promoters in *E. coli* to all possible combinations of four growth conditions could be predicted by linear superposition of temporal responses to individual conditions (Rothschild et al., 2014). Prediction of temporal expression dynamics during combination drug treatment from responses to individual drugs was also possible for 15 proteins in a human cancer cell line (Geva-Zatorsky et al., 2010). However, it is unclear if such simple interpolation or superposition principles for gene regulation in multidrug environments hold genome-wide and more generally across different prokaryotes and eukaryotes.

Quantitative measurements of gene expression changes in response to drugs are complicated by the fact that the growth rate change caused by the drugs alone can drastically affect gene expression (Brauer et al., 2008; Knijnenburg et al., 2009; Metzl-Raz et al., 2017; Regenberg et al., 2006), thus obfuscating any specific responses to the drugs. In a two-dimensional concentration gradient of two drugs, growth rate related changes alone can account for as much as three-quarters of the variance in gene expression (Bollenbach and Kishony, 2011). Further, analysis of yeast gene deletion mutants revealed that the most prominent gene expression change caused by the genetic perturbations was a general environmental-stress-response like signature associated with slower growth (O'Duibhir et al., 2014). Such non-specific effects due to growth rate changes are an underestimated challenge for the interpretation of gene expression measurements aiming to predict drug mechanisms and interactions.

Please cite this article in press as: Lukačišin and Bollenbach, Emergent Gene Expression Responses to Drug Combinations Predict Higher-Order Drug Interactions, Cell Systems (2019), https://doi.org/10.1016/j.cels.2019.10.004

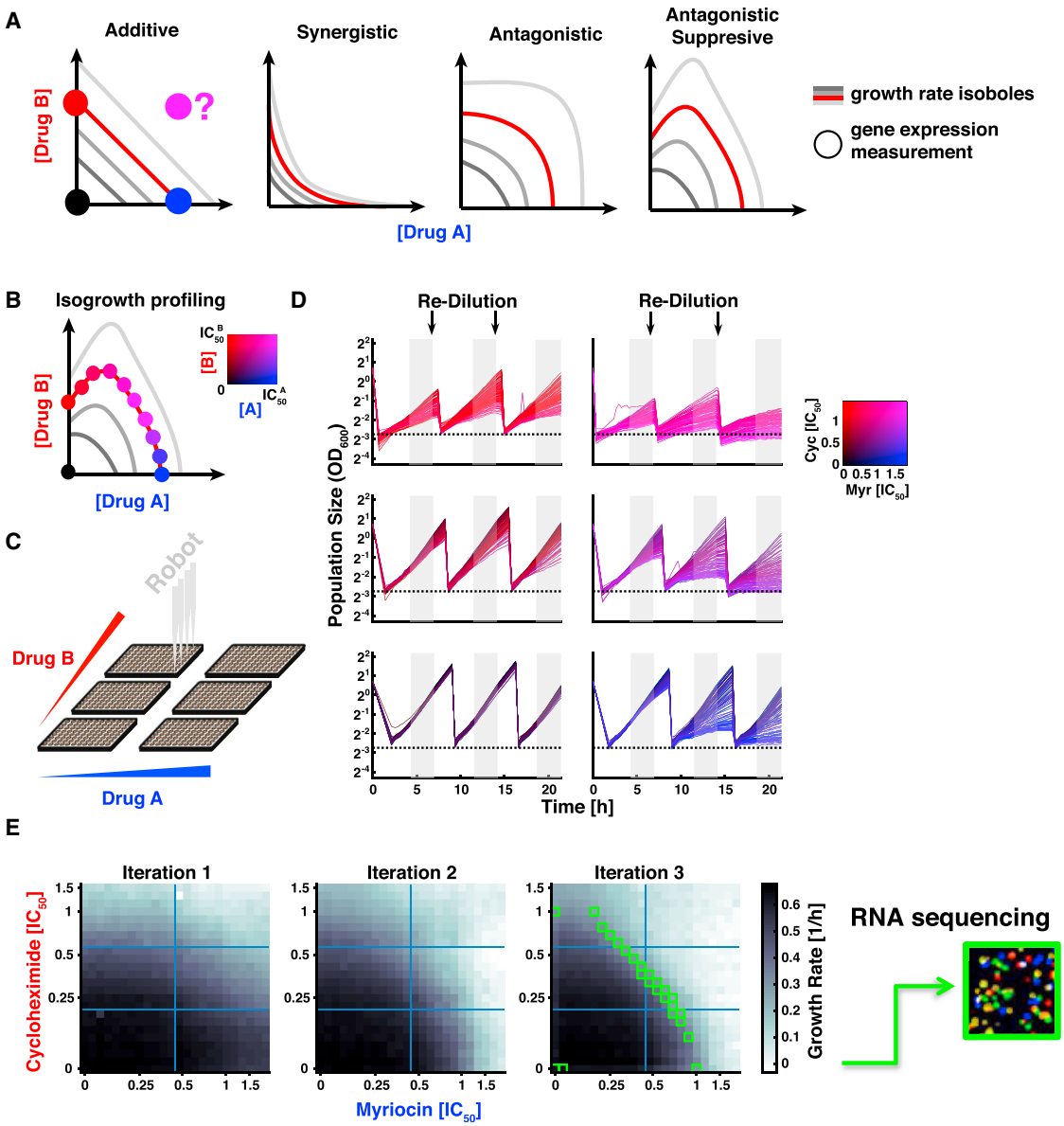

Figure 1. Automated Re-inoculation Protocol Allows for Steady-State Yeast Culture under Drug Combinations with Controlled Growth Rate and Cell Density

(A) Schematic diagrams of drug interactions based on Loewe additivity (Loewe, 1928). Lines show isoboles, i.e., lines of constant growth rate. Synergy, antagonism, and suppression are defined by the shape of the isoboles in comparison to the additive reference (left). To quantify gene expression changes due to drug combinations, gene expression measurements in no drug, the two individual drugs, and the drug combination should be performed (circles).

(B) Schematic illustration of the experimental strategy for isogrowth profiling. Gene expression is measured along a selected growth isobole at different ratios of the two drugs (circles, varying hue denotes varying ratio) to control for growth-rate-induced gene expression changes.

(C) Schematic illustration of how an automated system was used to produce a 24 × 24 discretized two-drug concentration gradient distributed over six 96-well microplates, to inoculate *S. cerevisiae*, and measure growth by optical density at 600 nm (OD_{600}).

(D) Growth measurements (OD_{600} over time) of yeast cells growing in a 2D-drug gradient of myriocin (Myr) and cycloheximide (Cyc). Drops in OD_{600} are the result of automated re-dilution, the dotted line denotes target OD_{600} directly after re-dilution. Shaded areas show regions used to determine the growth rates.

(E) Growth rates measured for the myriocin-cycloheximide 24 × 24 gradient after each of the three re-dilution steps. Green rectangles denote wells used to collect samples for RNA sequencing at the end of incubation. See Figure S1 for the growth rates and OD_{600} of the collected samples.

Here, we show that precise measurements of gene expression in drug combinations, which disentangle specific effects from growth-rate-induced changes, reveal emergent cellular responses to drug combinations, which in turn enable faithful predictions of three-way drug antagonism. To quantify gene expression changes in drug combinations independently of growth rate changes, we introduce a new methodology, isogrowth profiling, which is based on measurements at constant growth inhibition achieved by varying ratios of two drugs. Using this technique, we found that upregulation of cytoplasmic

Table 1. Information about Drugs Used in This Study

Drug	Abbr.	IC_{50} [μg/ml]	Mechanism of Action
Cycloheximide	Cyc	0.065	Inhibitor of cytosolic translation by binding to the large ribosomal subunit (Schneider-Poetsch et al., 2010)
Lithium Chloride	LiC	12×10^{3}	Pleiotropic; inhibits glycogen synthase kinase (O'Brien and Klein, 2009), Xrn1p endonuclease (Dichtl et al., 1997), phosphoglucomutase (Masuda et al., 2001), inositol monophosphatase (Lopez et al., 1999), protein degradation through the proteasome (Rice and Sartorelli, 2001), and other enzymes (Phiel and Klein, 2001)
Myriocin	Myr	0.50	Inhibitor of sphingolipid synthesis (Miyake et al., 1995), exacerbates the consequences of protein misfolding (Lee et al., 2011)
Rapamycin	Rap	6.8×10^{-3}	Inhibitor of nutrient-sensing TOR signaling (Crespo and Hall, 2002)

translation by the combination of lithium chloride and myriocin protected cells against the addition of the translation inhibitor cycloheximide; analogously, the upregulation of DNA integrity checkpoint by the combination of cycloheximide and myriocin protected cells against a DNA damaging agent. Thus, emergent regulatory responses to drug combinations enabled predicting higher-order drug interactions. We propose a readily applicable way of extending such growth-rate-controlled gene expression measurements to larger sets of drug combinations.

RESULTS

Automated Re-dilution Setup Enables Yeast Culture at Fixed Growth Inhibition by Two Drugs

We developed an automated method that precisely controls growth inhibition for microbial cultures growing in the presence of two drugs. This effort is necessary to keep gene expression measurements in the presence of different drugs comparable. It is challenging to keep growth inhibition constant both in individual drugs and drug combinations since the drug concentrations need to be quantitatively tuned according to the interactions of the specific drugs. We addressed this issue by culturing yeast populations in a fine-resolution 24 × 24 discretized concentration gradient of two drugs, i.e., 576 distinct two-drug concentrations spread over six 96-well microtitre plates (Figure 1C).

Given equal inoculum size, populations growing at the same growth rate would end up at the same cell density after a given incubation period. However, some drugs have a delayed effect on growth, allowing for faster growth at the beginning of incubation. As a result, gene expression measurements would be done at different cell density and nutrient content in the growth medium, which influences gene expression (Kolkman et al., 2006; Wu et al., 2004). We equalized the cell density by coupling our method with an automated re-inoculation protocol on a customized liquid handling robot, where all cultures are re-diluted to a fixed target population size (optical density) every 8 h (Figure 1D, STAR Methods). Three such re-dilution cycles are performed to ensure that populations undergo approximately eight generations at 50% growth inhibition, giving them sufficient time to reach a well-defined steady state of exponential growth while keeping the experimental expense manageable (Figure 1E). At the end of this procedure, we selected specific wells where the yeast populations grew at a defined growth rate for transcriptome analysis. These cultures have a narrow range of cell densities (Figure S1) and thus approximately the same nutrient content. Thus, we essentially sampled different drug ratios along a line of constant growth (isobole) in a two-drug concentration space, while controlling for cell density and nutrient content.

Isogrowth RNA-Sequencing in Drug Combinations Reveals Both Simple Interpolated and Emergent Gene Expression Changes

We used this re-dilution setup to measure genome-wide gene expression changes along growth isoboles for combinations of antifungal drugs ("isogrowth profiling"). We systematically investigated all pairwise combinations between four antifungal drugs. The drugs were selected such that their pairwise combinations included clear cases of antagonism, synergy, and additivity (Figure 1A); this selection thus enabled a systematic investigation of the utility of isogrowth profiling for characterizing drug interactions. We included the well-characterized drugs cycloheximide and rapamycin but also drugs with pleiotropic effects or unclear physiological roles, namely lithium chloride and myriocin (Table 1). Among the strongest drug interactions we observed are suppression of myriocin by lithium chloride and synergy between rapamycin and myriocin (Figure 2A); of note, the latter combination also has a synergistic effect with respect to aging (Huang et al., 2013, 2015). After three incubation cycles (~22 h), we extracted and sequenced the polyA-RNA from wells with a growth rate of ~50% relative to the no-drug reference (Figure 1E). To represent gene expression changes along the growth isobole, we parameterized the growth isobole by relative drug fraction (Figure 2B; STAR Methods). This representation has the advantage that the variation in contour length of the growth isobole due to drug interaction does not influence the visualization of the data.

Initial examination of gene expression changes along the growth isoboles revealed that genes often exhibit interpolating behavior in the drug combination, i.e., the gene expression level in the presence of both drugs at varying ratios was between the levels in each of the two drugs alone (Figure 2C left). An example of this behavior is given by LEU4, which codes for an enzyme that catalyzes the first step in leucine biosynthesis and is upregulated by rapamycin, which signals the presence of the nutrient-poor environment. Beyond simple interpolation, we detected genes that show emergent responses to the drug combination, i.e., their expression level in the combination is more extreme than in either drug alone (Figure 2C right). An example of this behavior are the COS2 and COS3 genes required for vesicular sorting and degradation of membrane proteins; these genes are upregulated in the combination only

Please cite this article in press as: Lukačišin and Bollenbach, Emergent Gene Expression Responses to Drug Combinations Predict Higher-Order Drug Interactions, Cell Systems (2019), https://doi.org/10.1016/j.cels.2019.10.004

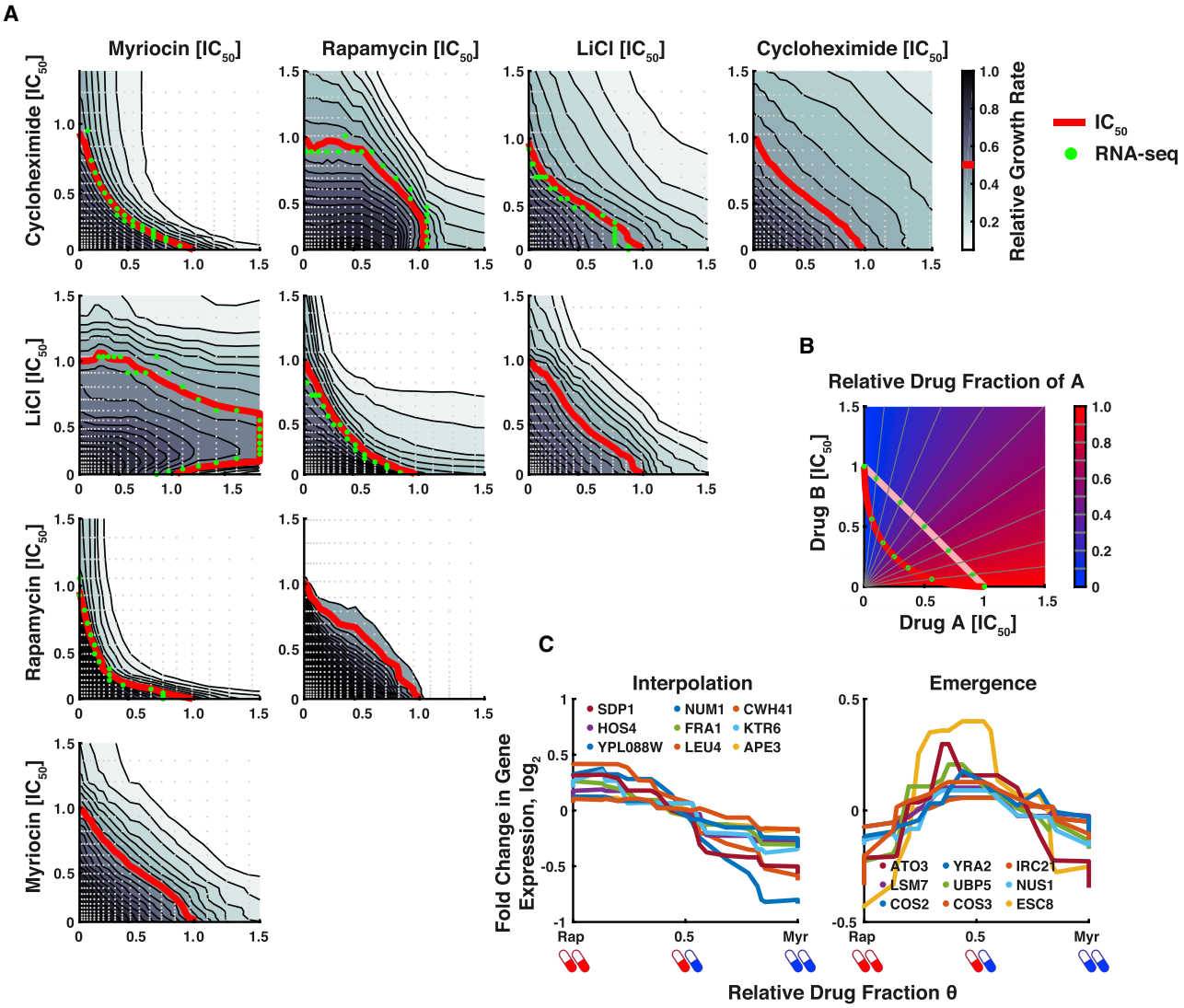

Figure 2. Selected Genes Responding to Pairwise Combinations of Interacting Antifungal Drugs Manifest Interpolating or Emergent Behavior

(A) Growth response surfaces for all pairwise combinations of four drugs (myriocin, rapamycin, lithium chloride, and cycloheximide). Growth rates were measured during the third iteration of the protocol shown in Figure 1. Black lines are isoboles; red line shows 50% growth inhibition isobole, gray dots indicate concentrations at which growth rate was measured, green dots indicate wells used for sample collection for RNA sequencing. Measured values are reported in Table S4.

(B) Schematic illustration of the definition of relative drug fraction θ used to reduce the dimensionality of the drug concentration space for visualizing gene expression changes along an isobole. The relative drug fraction is equivalent to the contour length of a projection of the points along the isobole onto the theoretical line of additivity (STAR Methods).

(C) Examples of gene expression changes along the 50% growth isobole for selected genes showing interpolating (left) and emergent (right) behavior in response to the rapamycin-myriocin combination. Gene expression is normalized to the no-drug control.

of rapamycin and myriocin, which increases chronological life span (Huang et al., 2013, 2015). Motivated by these observations, we systematically investigated the extent of interpolating and emergent gene expression responses in our genome-wide datasets.

Principal Component Analysis Decomposes Responses to Drug Combinations into Interpretable Contributions

To reveal general principles that relate responses to individual drugs to multidrug responses, we used principal component analysis (PCA), a dimensionality reduction method previously used to disentangle gene expression changes in drug combinations (Bollenbach and Kishony, 2011). This approach can reveal structure in the data, in particular, if the responses of most genes can be written as a linear superposition of relatively few characteristic response modes (principal components, PCs); it is not a *priori* clear though if this is possible. Using our dataset, we calculated the PCs of the global gene expression response along a growth rate isobole for each drug pair (STAR Methods). This analysis revealed that between 93% and 98% of the

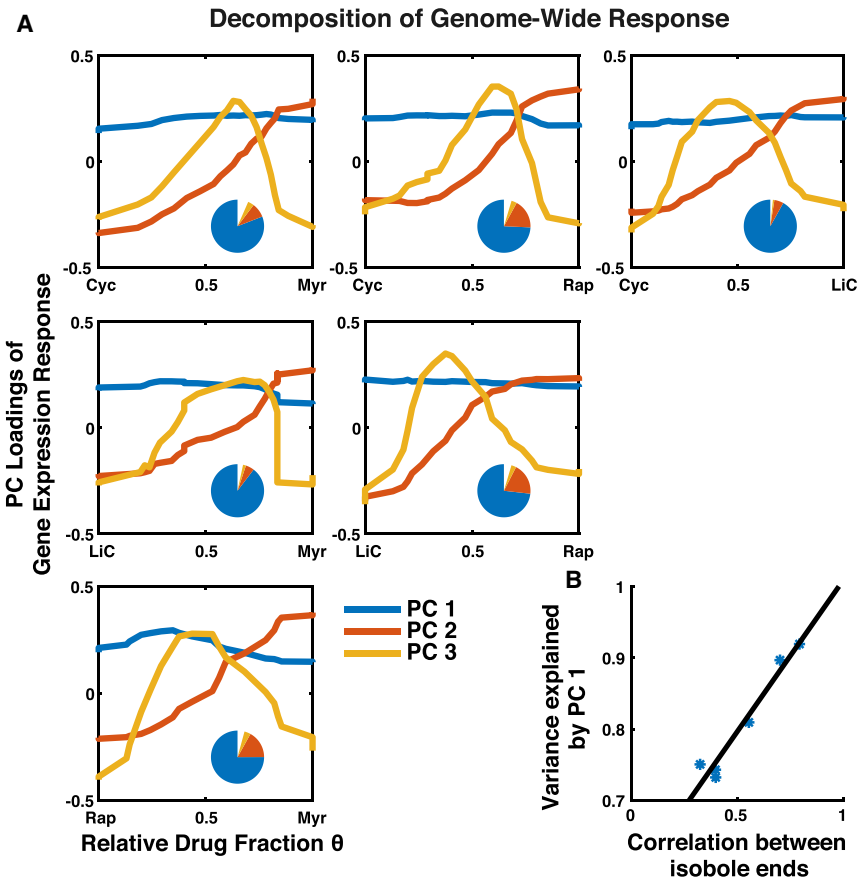

Figure 3. Gene Expression Responses to Drug Combinations Are a Superposition of Consensual, Drug-Specific, and Combination-Specific Effects

(A) First (blue), second (red), and third (yellow) principal component (PC) of genome-wide gene expression changes along the growth isoboles for the six drug combinations from Figure 2. PCA was performed for each drug combination separately (STAR Methods). Insets: pie charts showing a fraction of variance explained by these first three PCs.

(B) The fraction of variance explained by the first PC versus similarity of the responses to the individual drugs constituting the drug pair (quantified by Pearson's correlation coefficient) for all drug pairs in (A). Black line shows linear regression, $R^2 = 0.95$, $p = 9\times10^{-4}$ (t-statistic for the linear term). The first principal component explains an increasing fraction of the variance the more similar the effects of the drug pairs are.

variance in the dataset is explained by just three PCs, depending on the specific drug pair (Figure 3A). Notably, these first three PCs are similar across drug pairs, suggesting that each of these PCs has a common, potentially biologically meaningful origin.

For all drug pairs, the first PC was flat (blue lines in Figure 3A) and thus captures changes in gene expression relative to the no-drug reference that are independent of the drug ratio along the growth isobole. As this behavior is independent of the inhibiting drug, it reflects the global gene expression response to growth inhibition. The fact that the growth-rate-related first PC explains a considerable fraction of the gene expression variance under drug combinations further validates our experimental approach aimed at eliminating non-specific growth-rate effects. When the specific gene expression responses to the individual drugs are strongly correlated, the first PC additionally includes the common gene expression signatures of both drugs (Figure 3B).

The second PC captured how different gene expression responses to the individual drugs are typically interpolated (red lines in Figure 3A). Genes often respond differently to different drugs, which inevitably leads to conflicting responses in the presence of both drugs. The second PC exposes the default way in which genes that exhibit no specific response to the drug combination resolve such conflicts. The shape of the second PC was approximately linear, but sometimes clearly sigmoidal, in particular for the strongly antagonistic drug pair cycloheximide-rapamycin (Figure 3A). This result about genome-wide transcriptional regulation in a eukaryotic model system generalizes previous observations from bacteria that antagonistic drug interactions coincide with a sigmoidal interpolation ("prioritization") of gene expression conflicts, while additive combinations lead to a more linear interpolation ("averaging") (Bollenbach and Kishony, 2011). The large fraction of variance explained by the first two PCs implies that, for most yeast genes, the response to drug combinations is largely predictable from their responses to the individual drugs alone.

Our genome-wide dataset further enabled us to systematically identify emergent behaviors, where the expression of a gene under a drug combination is higher or lower than under either drug alone. For all drug pairs, such emergent responses were captured by the third PC (yellow lines in Figure 3A). Genes with a strong third PC are specifically up- or downregulated in the presence of both drugs due to effects that are absent in either drug alone. Based on the observed shapes of the PCs, we hypothesized that functional analysis of genes governed strongly by the second and third principal component should yield testable predictions about the specific effects of individual drugs and drug interactions on cell physiology, respectively.

Analysis of Specific Drug Effects Reveals that Myriocin Prepares Yeast for Respiratory Medium

We first exploited our dataset to extract the specific effects of individual drug perturbations on cell physiology. Because of the confounding effects of growth inhibition, this cannot be achieved by simple comparisons of gene expression measurements in the presence and absence of a drug alone. This problem is particularly evident for the abundances of ribosomes and mitochondria, which are strongly affected by growth rate (Metzl-Raz et al., 2017). Therefore, we leveraged the fact that, by construction, the second PC is orthogonal to the first PC, which captures the non-specific growth rate effect. The second

Please cite this article in press as: Lukačišin and Bollenbach, Emergent Gene Expression Responses to Drug Combinations Predict Higher-Order Drug Interactions, Cell Systems (2019), https://doi.org/10.1016/j.cels.2019.10.004

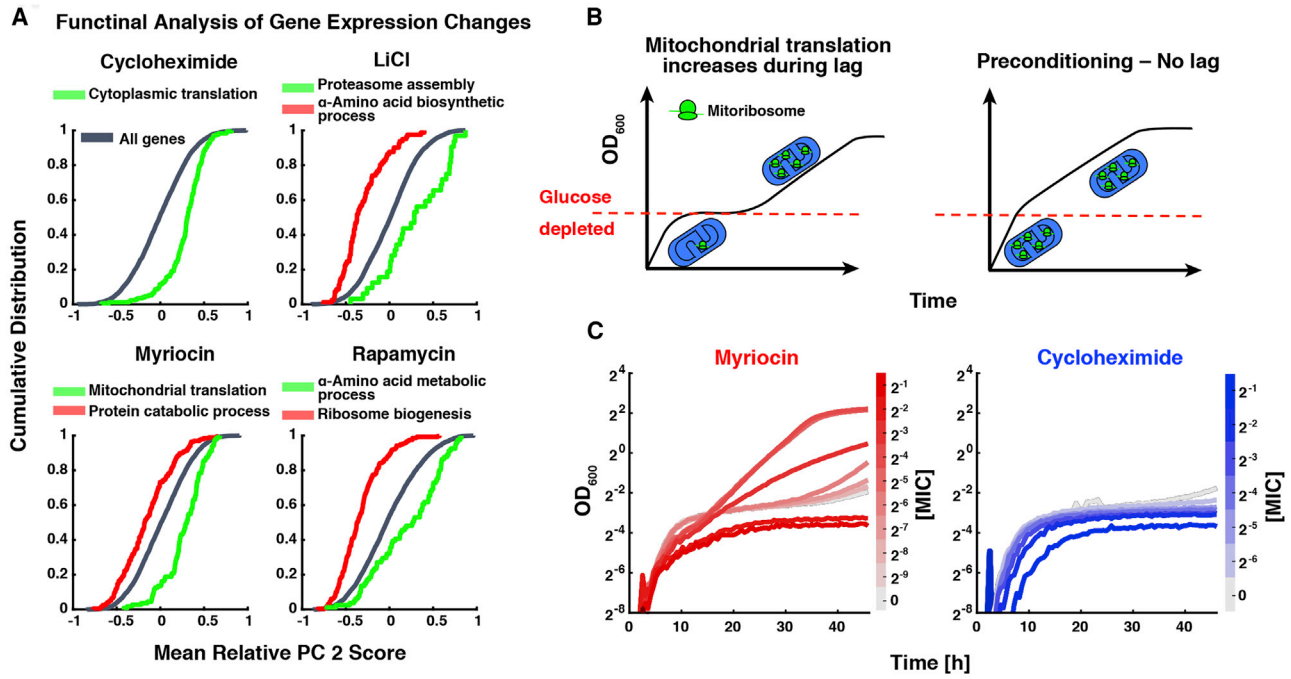

Figure 4. Functional Analysis of Genes with Interpolating Behavior Reveals Specific Effects of Individual Drugs on Cell Physiology

(A) Cumulative distributions of mean relative second PC scores for individual genes across experiments for the respective drug (STAR Methods). Before averaging, the scores were inverted if needed, such that positive scores always indicate upregulation in the given drug. Cellular functions that are enriched based on gene ontology (GO) analysis of up- and downregulated genes are highlighted in green and red, respectively. The most significant GO term that has no offspring (more specific) term with $p \leq 10^{-9}$ is displayed (STAR Methods). For cycloheximide, no functional group was found to be enriched for downregulation at the chosen level of significance. See also Table S1.

(B) Schematics of hypothetical growth curves during diauxic shifts from fermentation to respiration: the diauxic lag (left) should be shortened if the mitochondrial translation is induced while still in fermentative medium (right).

(C) Growth curves of yeast cultured in YPG glycerol medium inoculated from glucose overnight culture at different concentrations of myriocin (left) and cycloheximide (right). Intermediate myriocin concentrations drastically shorten the diauxic lag time; in contrast, the control drug cycloheximide has no effect on diauxic lag. MIC = Minimum Inhibitory Concentration, 2.5 μg/ml for myriocin, 0.16 μg/ml for cycloheximide.

PC, which monotonically interpolates between the individual drug responses, can be used to rigorously identify specific responses of genes to individual drugs. To this end, we quantified the fraction of variance in expression along the two-drug isobole that is explained by the second PC for each gene. To identify the gene expression change that can be specifically attributed to a given drug, we averaged this fraction across all experiments involving that drug, accounting for the sign of the expression change (STAR Methods). This procedure does not necessarily average out the entire contribution of the other drugs and, due to inherent limitations of PCA, it might not capture more complex behaviors of smaller gene groups. Nevertheless, it estimates the specific effect of a single drug on gene expression more thoroughly than a simple comparison to a single reference condition. We then sorted the genes according to this average and performed gene ontology enrichment analysis (STAR Methods). This procedure produces a list of functional gene groups that are specifically up- or downregulated in response to each drug in a way that is not obfuscated by growth rate changes or any other non-specific effects of drugs.

The most strongly enriched up- and downregulated functional gene groups in the cellular response to individual drugs confirmed expectations in the light of published literature (Figure 4A; Tables 1 and S1). Cycloheximide, a drug that binds to the large ribosomal subunit (Schneider-Poetsch et al., 2010) and is commonly used to inhibit cytosolic translation, elicited upregulation of genes involved in cytoplasmic translation (Figure 4A). Rapamycin, a specific inhibitor of nutrient-sensing TOR signaling (Crespo and Hall, 2002), triggered a decrease in ribosome biogenesis and an increase in amino acid biosynthesis (Figure 4A)—canonical responses to low-nutrient environments (Mayer and Grummt, 2006; Peng et al., 2002). The pleiotropic drug lithium chloride led to upregulation of proteasome assembly with a concomitant decrease in amino acid biosynthesis (Figure 4A). Both observations are consistent with a cellular response to the inhibition of protein degradation—a plausible effect as lithium chloride is known to inhibit protein degradation through the proteasome (Rice and Sartorelli, 2001) along with inhibition of other enzymes (Table 1). Together, these results corroborate that our analysis of the second PC can identify specific cellular responses to individual drugs and thus provide insights into drug modes of action.

Furthermore, this analysis exposed previously unreported effects of individual drugs. We found that myriocin, a known inhibitor of sphingolipid synthesis (Miyake et al., 1995), leads to an increase in mitochondrial translation and downregulation of protein degradation. The latter is consistent with previous reports that myriocin exacerbates the consequences of protein

misfolding (Lee et al., 2011). However, the effect of myriocin on mitochondrial translation was entirely unexpected. Therefore, we performed additional experiments to test the prediction that the upregulation of mitochondrial translation is one of the major physiological effects of myriocin.

We reasoned that the mitochondrial ribosome primarily translates genes needed for oxidative metabolism (Couvillion et al., 2016). Therefore, the increased mitoribosome expression should increase respiratory capacity, especially in conditions where this capacity is not maximal to begin with, e.g., during fermentative overflow metabolism in glucose. Thus, we hypothesized that the mitoribosome overexpression triggered by myriocin treatment should have a growth rate cost on a fermentative carbon source, but should shorten the diauxic lag upon a shift to an oxidative carbon source such as glycerol (Figure 4B). Indeed, intermediate concentrations of myriocin drastically shortened this diauxic lag, while higher doses led to more pronounced inhibition of fermentative growth (Figure 4C). Inhibition by a control drug (cycloheximide) supported that the shortening of the diauxic lag was not due to a non-specific decrease in growth rate, but rather due to specific effects of myriocin, confirming the prediction of our analysis based on the second PC. Overall, these results show that abstracting growth rate effects from the specific gene expression changes triggered by individual drugs can reveal far-reaching changes in cellular physiology and metabolism.

Emergent Response to Drug Combinations Predicts Antagonisms with Drugs Targeting Upregulated Pathways

We next sought to identify the physiological consequences of drug combinations that go qualitatively beyond those brought about by the constituent drugs alone. We reasoned that functional analysis of the genes strongly governed by the third PC should expose the emergent effects of the two drugs on cell physiology, even if these genes are also affected by growth rate or by the individual drugs alone. To identify the emergent effects of each drug combination, we sorted the genes by their third PC score and, after accounting for the sign of the third PC, performed gene ontology enrichment analysis (STAR Methods). This procedure revealed functional groups (Tables S2 and S3) that showed significant emergent upregulation (for five drug pairs) or downregulation (for two drug pairs, Figure S2). In particular, a DNA replication checkpoint showed an emergent response to the myriocin-cycloheximide combination (Figure S2). Similarly, myriocin and lithium chloride together triggered a specific increase in ribosome biogenesis. Our analysis thus identified cellular functions that specifically respond to the drug combinations.

To validate this analysis and explore its utility, we made specific testable predictions based on the identified emergent gene regulation. We reasoned that the upregulation of functional groups of genes in response to drug combinations may not always be adaptive. If upregulation is non-adaptive, it could create a buffer for the cell when exposed to a third drug that inhibits the upregulated pathway, rendering the cell less sensitive to the third drug (Figure 5A). In other words, this would lead to three-way drug antagonism. To test this idea, we added the DNA damaging agent methyl methanesulfonate (MMS) on top of the myriocin-cycloheximide combination, since the myriocin-cycloheximide combination on its own triggered emergent upregulation of a DNA replication checkpoint (Figure 5B). Indeed, the addition of this third compound inverted the synergism between myriocin and cycloheximide to antagonism (Figure 5C). Similarly, adding the translation inhibitor cycloheximide on top of the myriocin-lithium chloride combination, which triggered an emergent increase in ribosome synthesis (Figure 5B), strongly amplified antagonism (Figure 5D). These results suggest that emergent gene regulation in response to drug combinations, identified upon proper accounting for non-specific effects and individual drug effects, often enables faithful predictions of higher-order interactions with additional drugs.

Emergent Responses to Drug Combinations Should Be Measured Where the Drug Interaction Is Strongest

While this functional analysis of the third PC is valuable for characterizing the specific effects of drug combinations, this approach is relatively hard to utilize: our gene expression measurements along the two-drug growth isobole (Figures 1 and 2) require feedback-controlled liquid handling and are not readily scalable to larger numbers of drug pairs. Therefore, we aimed to establish a more accessible protocol that provides comparable information on emergent gene regulation under drug combinations at a lower experimental effort. To identify genes strongly governed by the third PC, it would in principle suffice to measure gene expression in the presence of the individual drugs alone (i.e., at both ends of the isoboles) and at one point in drug concentration space in the middle of the isobole, where both drugs are present. The ideal choice for the latter would be the point in drug combination space where the third PC has its peak, as this point can provide maximum information about emergent gene expression. We asked whether such a point on the isobole could be identified without measuring the gene expression along the entire isobole.

We observed that the peak of the third PC generally coincides well with the point in drug space where the deviation of growth rate from the additive expectation is most pronounced (Figures 6A and S3). In other words, the third PC is maximal at the drug ratio where the drug interaction is strongest. This observation exposes a simple, yet powerful principle for gaining maximum information from a single gene expression measurement under a drug combination: such measurements should be performed at drug concentrations where the growth rate deviates maximally from the additive expectation (Figures 6B and S4)—a point that is readily identified from a standard growth-rate-response surface measurement.

DISCUSSION

Understanding the principles that govern gene expression responses to multiple drugs can facilitate the design of new combination therapies. However, measurements of gene expression responses to drugs are obfuscated by changes in growth rate (Bollenbach and Kishony, 2011; O'Duibhir et al., 2014). We found that at least 75% of all variations in gene expression in yeast responding to combinations of two drugs can be attributed simply to changes in growth rate. Thus, we introduced isogrowth profiling, a framework for measuring gene expression changes

Please cite this article in press as: Lukačišin and Bollenbach, Emergent Gene Expression Responses to Drug Combinations Predict Higher-Order Drug Interactions, Cell Systems (2019), https://doi.org/10.1016/j.cels.2019.10.004

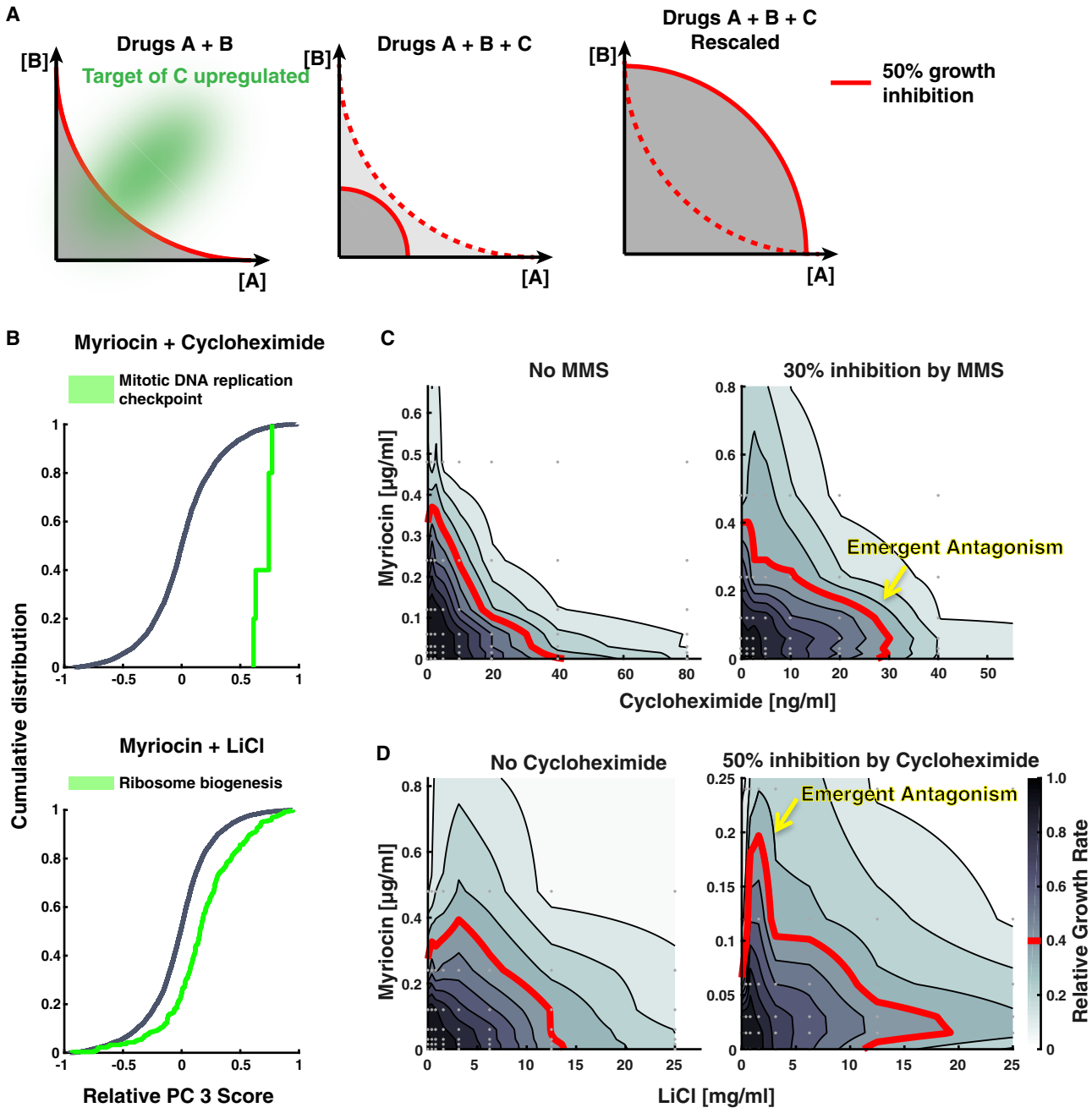

Figure 5. Cellular Functions Showing Emergent Responses to Drug Combinations Enable Predictions of Higher-Order Drug Interactions

(A) Schematic: non-adaptive upregulation of gene expression in response to the combination of two drugs (left; green shading) may protect against a third drug targeting the upregulated pathway (middle) and thus lead to higher-order antagonism (right panel). The solid red line is the 50% growth rate isobole in each condition, the dashed red line shows a 50% growth rate isobole in the absence of drug C for comparison.

(B) Cumulative distribution functions of relative third PC scores for individual genes for the drug combinations shown in C (top) and D (bottom). Cellular functions that are enriched based on gene ontology (GO) analysis of upregulated genes are highlighted in green; only the most significant GO term that has no offspring (more specific) term with $p \leq 10^{-6}$ is shown (STAR Methods). For other drug pairs, see Figure S2 and Tables S2 and S3.

(C) Dose-response surfaces for the myriocin-cycloheximide combination in the absence (left) and in the presence (right) of the DNA damaging agent methyl methanesulfonate (MMS). The interaction is modified by a third drug targeting the pathway upregulated in the two-drug combination: MMS inverts synergism between myriocin and cycloheximide into antagonism. Growth rates are normalized to the growth rates in the absence of both myriocin and cycloheximide.

(D) Ribosomal inhibitor cycloheximide increases antagonism between myriocin and LiCl, leading to strong suppression. Yellow arrows highlight the change to stronger antagonism. Growth rates are normalized to the growth rates in the absence of both myriocin and LiCl. Measured values are reported in Table S5.

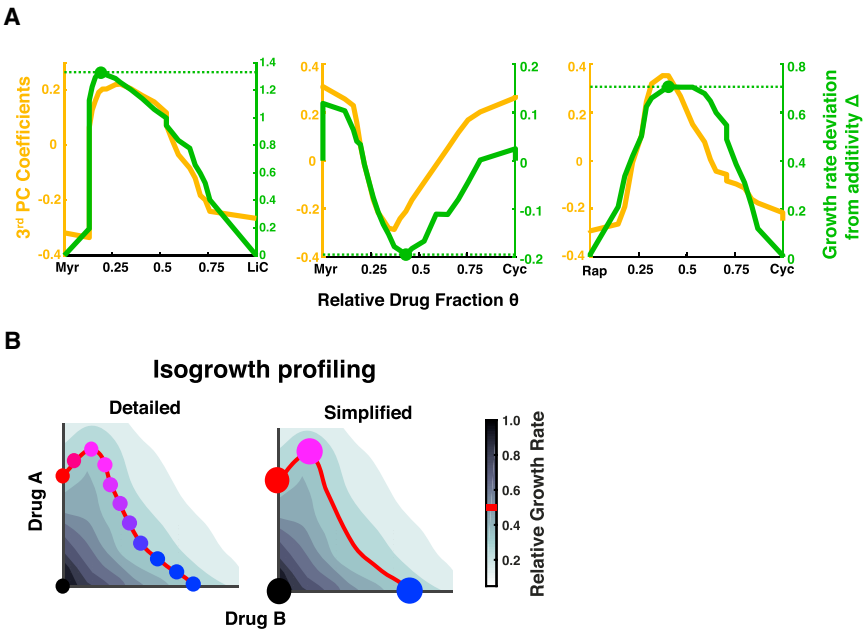

Figure 6. Gene Expression Responses to Drug Combinations Yield Maximum Information at Drug Concentrations that Deviate Maximally from Additivity

(A) Third PC as in Figure 3A (yellow) and deviation of growth isobole from theoretical additivity line (green; see Figure S3 for definition) for selected drug pairs. Green dot labels the point of maximum deviation. For other drug pairs, see Figure S3.

(B) Schematic of detailed (left) versus simplified (right) isogrowth profiling: in the simplified version, the effects of single drugs are measured at the same growth rate (red and blue circles), but only a single measurement is performed in the presence of both drugs, at the point in two-drug space where the drug interaction is maximum (magenta circle). See also Figures S4 and S5 for the justification of the choice of measurement points.

in drug combinations while keeping growth rate constant (Figure 2). Beyond growth effects, most of the gene expression variance is well approximated by interpolating the responses to the individual drugs (Figure 3). These data corroborate the view that regulatory responses to drug combinations are largely predictable from the responses to the constituent drugs, as previously observed in prokaryotes and in human cells (Bollenbach and Kishony, 2011; Geva-Zatorsky et al., 2010).

We found that some genes show emergent responses to drug combinations. Even though these genes contribute little to global gene expression variance, they are likely responsible for key phenomena caused by drug combinations that are otherwise hard to rationalize. Identifying cellular functions that show emergent responses enabled us to predict antagonisms with a third drug (Figure 5). Our growth-rate-controlled experiment enabled abstracting both growth-rate-dependent and drug-specific gene expression changes from emergent drug-combination-specific changes even for highly growth-rate-dependent genes, such as ribosomal genes. In this way, we discovered emergent responses that would otherwise be masked by strong growth-rate-dependent effects (Figure S5). In particular, the combination of myriocin and cycloheximide caused upregulation of a DNA replication checkpoint, protecting the cells from a DNA damaging agent as predicted; similarly, the combination of lithium chloride and myriocin upregulated cytoplasmic ribosomes and protected cells from a translation inhibitor (Figure 5). We identified various other emergent responses (Tables S2 and S3). In many cases, the higher-order antagonisms predicted based on these observations cannot be easily tested because drugs targeting the upregulated pathway are unavailable. For example, the functional consequences of upregulating vesicular trafficking in the combination of myriocin and rapamycin would have to be tested by other assays. Our results suggest that emergent gene regulation under drug pairs often singles out cellular functions at the heart of higher-order drug interactions.

Recent work suggested that growth rates in higher-order drug cocktails may be largely predictable from the pairwise interactions between the constituent drugs (Wood et al., 2012; Zimmer et al., 2016, 2017). However, true higher-order drug interactions also seem common (Tekin et al., 2018). Our results indicate that emergent gene expression responses to pairwise drug interactions enable predictions of such higher-order interactions. Why is that so? Yeast evolved to respond to stresses it frequently encounters in its natural environment. During the course of evolution, stress caused by drugs targeting specific parts of the cellular machinery was probably rare compared to changes in nutrient availability, temperature, pH, etc. Thus, yeast may not have adaptive responses to all specific stresses caused by drugs, and this seems even less likely for combinatorial stressors. Hence, drug combinations likely trigger non-adaptive gene expression changes, which do not increase fitness. In other words, the emergent regulation of specific pathways under drug combinations is likely caused indirectly by a regulatory machinery that evolved for other purposes (Price et al., 2013). The non-adaptive emergent upregulation of a cellular pathway in response to a drug pair can create a "buffer" against the action of a third drug that inhibits the upregulated pathway, or, conversely, a susceptibility for a drug that requires the upregulated pathway for its action.

Isogrowth profiling can identify detailed effects of individual drugs and drug combinations on cell physiology, which can be used to predict certain three-way drug interactions. While we focused on a single model organism and a limited number of drugs, we anticipate that the basic principles uncovered here are more broadly applicable to other systems and drugs. However, isogrowth profiling requires a large number of gene expression measurements. To increase its applicability, we propose a simplified version that requires measuring gene expression at only four well-chosen points in two-dimensional drug concentration space, where the drug interaction is maximal while the overall inhibitory effect is kept constant (Figure 6). This simplified framework provides almost complete information on emergent gene regulation (Figure S4) and facilitates systematic investigations of gene expression responses for all pairwise

Please cite this article in press as: Lukačišin and Bollenbach, Emergent Gene Expression Responses to Drug Combinations Predict Higher-Order Drug Interactions, Cell Systems (2019), https://doi.org/10.1016/j.cels.2019.10.004

combinations of larger sets of drugs. This approach should, in principle, not be limited to drugs that inhibit growth but extendable to inhibitors of any cellular function as long as the inhibitory effect can be quantified. A large-scale characterization of the emergent physiological changes under drug combinations using the approach introduced here has the potential to inform predictive algorithms for the design of advanced multidrug therapies.

Key Changes Prompted by Reviewers Comments

In response to reviewers comments, the discussion was slightly modified to better reflect that the current study is limited to a single model organism and a few drugs. Further, an explicit mention of the limitations of PCA with respect to discovering responses caused by a small number of genes was added. A more detailed explanation of the evolutionary argument that responses to combinatorial drug perturbations are likely non-adaptive was also included. For context, the complete Transparent Peer Review Record is included within the Supplemental Information.

STAR★METHODS

Detailed methods are provided in the online version of this paper and include the following:

- KEY RESOURCES TABLE
- LEAD CONTACT AND MATERIALS AVAILABILITY
- EXPERIMENTAL MODEL AND SUBJECT DETAILS
- METHOD DETAILS
  - Automated Re-inoculation Setup for Reproducible Yeast Culture
  - RNA Extraction and Sequencing
  - Diauxic Shift Measurements
  - Three-Drug Interaction Measurements
- QUANTIFICATION AND STATISTICAL ANALYSIS
- DATA AND CODE AVAILABILITY

SUPPLEMENTAL INFORMATION

Supplemental Information can be found online at https://doi.org/10.1016/j.cels.2019.10.004.

ACKNOWLEDGMENTS

We would like to thank Marta Lukačišinová and the IST Austria Life Sciences Facility for the support of the automated liquid handling system. Naama Barkai and Miri Carmi for help with the sequencing library preparation protocol. Blagovesta Popova, Gerhard Braus, and Jürgen Dohmen for providing strains for experiments that were not included in the final version of the manuscript. Hania Köver and Nick Barton for organizational support. Mike Springer, Daria Siekhaus, Gašper Tkačik, Roy Kishony, Murat Cokol, and the members of the Bollenbach group for useful discussions and Kevin Wood, Mike Springer, Alex Ng, and Yuval Mulla for the critical reading of the manuscript. This work was supported in part by the Austrian Science Fund (FWF) standalone grant P 27201-B22, HFSP program grant no. RGP0042/2013, and German Research Foundation (DFG) Collaborative Research Centre (SFB) 1310.

AUTHOR CONTRIBUTIONS

Conceptualization, M.L. and T.B.; Investigation, M.L.; Formal Analysis, M.L.; Data Curation, M.L.; Writing, M.L. and T.B.; Resources, T.B.; Visualization, M.L.; Supervision, T.B.; Project Administration, T.B.; and Funding Acquisition, T.B.

DECLARATION OF INTERESTS

The authors declare no competing interests.

Received: August 16, 2019
Revised: October 3, 2019
Accepted: October 11, 2019
Published: November 13, 2019

REFERENCES

Bar-Ziv, R., Voichek, Y., and Barkai, N. (2016). Chromatin dynamics during DNA replication. Genome Res. *26*, 1245–1256.

Bollenbach, T. (2015). Antimicrobial interactions: mechanisms and implications for drug discovery and resistance evolution. Curr. Opin. Microbiol. *27*, 1–9.

Bollenbach, T., and Kishony, R. (2011). Resolution of gene regulatory conflicts caused by combinations of antibiotics. Mol. Cell *42*, 413–425.

Brauer, M.J., Huttenhower, C., Airoldi, E.M., Rosenstein, R., Matese, J.C., Gresham, D., Boer, V.M., Troyanskaya, O.G., and Botstein, D. (2008). Coordination of growth rate, cell cycle, stress response, and metabolic activity in yeast. Mol. Biol. Cell *19*, 352–367.

Brochado, A.R., Telzerow, A., Bobonis, J., Banzhaf, M., Mateus, A., Selkrig, J., Huth, E., Bassler, S., Zamarreño Beas, J., Zietek, M., et al. (2018). Species-specific activity of antibacterial drug combinations. Nature *559*, 259–263.

Chen, S.H., and Lahav, G. (2016). Two is better than one; toward a rational design of combinatorial therapy. Curr. Opin. Struct. Biol. *41*, 145–150.

Chevereau, G., and Bollenbach, T. (2015). Systematic discovery of drug interaction mechanisms. Mol. Syst. Biol. *11*, 807.

Cohen, A.A., Geva-Zatorsky, N., Eden, E., Frenkel-Morgenstern, M., Issaeva, I., Sigal, A., Milo, R., Cohen-Saidon, C., Liron, Y., Kam, Z., et al. (2008). Dynamic proteomics of individual cancer cells in response to a drug. Science *322*, 1511–1516.

Cokol, M., Chua, H.N., Tasan, M., Mutlu, B., Weinstein, Z.B., Suzuki, Y., Nergiz, M.E., Costanzo, M., Baryshnikova, A., Giaever, G., et al. (2011). Systematic exploration of synergistic drug pairs. Mol. Syst. Biol. *7*, 544.

Cokol, M., Weinstein, Z.B., Yilancioglu, K., Tasan, M., Doak, A., Cansever, D., Mutlu, B., Li, S., Rodriguez-Esteban, R., Akhmedov, M., et al. (2014). Large-scale identification and analysis of suppressive drug interactions. Chem. Biol. *21*, 541–551.

Cokol, M., Kuru, N., Bicak, E., Larkins-Ford, J., and Aldridge, B.B. (2017). Efficient measurement and factorization of high-order drug interactions in Mycobacterium tuberculosis. Sci. Adv. *3*, e1701881.

Couvillion, M.T., Soto, I.C., Shipkovenska, G., and Churchman, L.S. (2016). Synchronized mitochondrial and cytosolic translation programs. Nature *533*, 499–503.

Crespo, J.L., and Hall, M.N. (2002). Elucidating TOR signaling and rapamycin action: lessons from Saccharomyces cerevisiae. Microbiol. Mol. Biol. Rev. *66*, 579–591.

Dichtl, B., Stevens, A., and Tollervey, D. (1997). Lithium toxicity in yeast is due to the inhibition of RNA processing enzymes. EMBO J. *16*, 7184–7195.

Eden, E., Navon, R., Steinfeld, I., Lipson, D., and Yakhini, Z. (2009). GOrilla: a tool for discovery and visualization of enriched GO terms in ranked gene lists. BMC Bioinformatics *10*, 48.

Fischbach, M.A. (2011). Combination therapies for combating antimicrobial resistance. Curr. Opin. Microbiol. *14*, 519–523.

Geva-Zatorsky, N., Dekel, E., Cohen, A.A., Danon, T., Cohen, L., and Alon, U. (2010). Protein dynamics in drug combinations: a linear superposition of individual-drug responses. Cell *140*, 643–651.

Huang, X., Liu, J., Withers, B.R., Samide, A.J., Leggas, M., and Dickson, R.C. (2013). Reducing signs of aging and increasing lifespan by drug synergy. Aging Cell *12*, 652–660.

Huang, X., Leggas, M., and Dickson, R.C. (2015). Drug synergy drives conserved pathways to increase fission yeast lifespan. PLoS One *10*, e0121877.

Kim, D., Pertea, G., Trapnell, C., Pimentel, H., Kelley, R., and Salzberg, S.L. (2013). TopHat2: accurate alignment of transcriptomes in the presence of insertions, deletions and gene fusions. Genome Biol. *14*, R36.

Knijnenburg, T.A., Daran, J.M., van den Broek, M.A., Daran-Lapujade, P.A., de Winde, J.H., Pronk, J.T., Reinders, M.J., and Wessels, L.F. (2009). Combinatorial effects of environmental parameters on transcriptional regulation in Saccharomyces cerevisiae: a quantitative analysis of a compendium of chemostat-based transcriptome data. BMC Genomics *10*, 53.

Kolkman, A., Daran-Lapujade, P., Fullaondo, A., Olsthoorn, M.M.A., Pronk, J.T., Slijper, M., and Heck, A.J.R. (2006). Proteome analysis of yeast response to various nutrient limitations. Mol. Syst. Biol. *2*, 2006.0026.

Lee, Y.J., Wang, S., Slone, S.R., Yacoubian, T.A., and Witt, S.N. (2011). Defects in very long chain fatty acid synthesis enhance alpha-synuclein toxicity in a yeast model of Parkinson's disease. PLoS One *6*, e15946.

Liao, Y., Smyth, G.K., and Shi, W. (2014). featureCounts: an efficient general purpose program for assigning sequence reads to genomic features. Bioinformatics *30*, 923–930.

Loewe, S. (1928). Die quantitativen Probleme der Pharmakologie. Ergeb. Physiol. *27*, 47–187.

Lopez, F., Leube, M., Gil-Mascarell, R., Navarro-Aviñó, J.P., and Serrano, R. (1999). The yeast inositol monophosphatase is a lithium- and sodium-sensitive enzyme encoded by a non-essential gene pair. Mol. Microbiol. *31*, 1255–1264.

Masuda, C.A., Xavier, M.A., Mattos, K.A., Galina, A., and Montero-Lomelí, M. (2001). Phosphoglucomutase is an in vivo lithium target in yeast. J. Biol. Chem. *276*, 37794–37801.

Mayer, C., and Grummt, I. (2006). Ribosome biogenesis and cell growth: mTOR coordinates transcription by all three classes of nuclear RNA polymerases. Oncogene *25*, 6384–6391.

Metzl-Raz, E., Kafri, M., Yaakov, G., Soifer, I., Gurvich, Y., and Barkai, N. (2017). Principles of cellular resource allocation revealed by condition-dependent proteome profiling. eLife *6*, e28034.

Miyake, Y., Kozutsumi, Y., Nakamura, S., Fujita, T., and Kawasaki, T. (1995). Serine palmitoyltransferase is the primary target of a sphingosine-like immunosuppressant, ISP-1/myriocin. Biochem. Biophys. Res. Commun. *211*, 396–403.

Molinelli, E.J., Korkut, A., Wang, W., Miller, M.L., Gauthier, N.P., Jing, X., Kaushik, P., He, Q., Mills, G., Solit, D.B., et al. (2013). Perturbation biology: inferring signaling networks in cellular systems. PLoS Comput. Biol. *9*, e1003290.

O'Brien, W.T., and Klein, P.S. (2009). Validating GSK3 as an in vivo target of lithium action. Biochem. Soc. Trans. *37*, 1133–1138.

O'Duibhir, E., Lijnzaad, P., Benschop, J.J., Lenstra, T.L., van Leenen, D., Groot Koerkamp, M.J.G., Margaritis, T., Brok, M.O., Kemmeren, P., and Holstege, F.C. (2014). Cell cycle population effects in perturbation studies. Mol. Syst. Biol. *10*, 732.

Pemovska, T., Bigenzahn, J.W., and Superti-Furga, G. (2018). Recent advances in combinatorial drug screening and synergy scoring. Curr. Opin. Pharmacol. *42*, 102–110.

Peng, T., Golub, T.R., and Sabatini, D.M. (2002). The immunosuppressant rapamycin mimics a starvation-like signal distinct from amino acid and glucose deprivation. Mol. Cell. Biol. *22*, 5575–5584.

Phiel, C.J., and Klein, P.S. (2001). Molecular targets of lithium action. Annu. Rev. Pharmacol. Toxicol. *41*, 789–813.

Price, M.N., Deutschbauer, A.M., Skerker, J.M., Wetmore, K.M., Ruths, T., Mar, J.S., Kuehl, J.V., Shao, W., and Arkin, A.P. (2013). Indirect and suboptimal control of gene expression is widespread in bacteria. Mol. Syst. Biol. *9*, 660.

Regenberg, B., Grotkjaer, T., Winther, O., Fausbøll, A., Åkesson, M., Bro, C., Hansen, L.K., Brunak, S., and Nielsen, J. (2006). Growth-rate regulated genes have profound impact on interpretation of transcriptome profiling in Saccharomyces cerevisiae. Genome Biol. *7*, R107.

Rice, A.M., and Sartorelli, A.C. (2001). Inhibition of 20 S and 26 S proteasome activity by lithium chloride: impact on the differentiation of leukemia cells by all-trans-retinoic acid. J. Biol. Chem. *276*, 42722–42727.

Rothschild, D., Dekel, E., Hausser, J., Bren, A., Aidelberg, G., Szekely, P., and Alon, U. (2014). Linear superposition and prediction of bacterial promoter activity dynamics in complex conditions. PLoS Comput. Biol. *10*, e1003602.

Russ, D., and Kishony, R. (2018). Additivity of inhibitory effects in multidrug combinations. Nat. Microbiol. *3*, 1339–1345.

Schneider-Poetsch, T., Ju, J., Eyler, D.E., Dang, Y., Bhat, S., Merrick, W.C., Green, R., Shen, B., and Liu, J.O. (2010). Inhibition of eukaryotic translation elongation by cycloheximide and lactimidomycin. Nat. Chem. Biol. *6*, 209–217.

Smith, T., Heger, A., and Sudbery, I. (2017). UMI-tools: modeling sequencing errors in Unique Molecular Identifiers to improve quantification accuracy. Genome Res. *27*, 491–499.

Tekin, E., Beppler, C., White, C., Mao, Z., Savage, V.M., and Yeh, P.J. (2016). Enhanced identification of synergistic and antagonistic emergent interactions among three or more drugs. J. R. Soc. Interface *13*, 20160332.

Tekin, E., White, C., Kang, T.M., Singh, N., Cruz-Loya, M., Damoiseaux, R., Savage, V.M., and Yeh, P.J. (2018). Prevalence and patterns of higher-order drug interactions in Escherichia coli. NPJ Syst. Biol. Appl. *4*, 31.

Wood, K., Nishida, S., Sontag, E.D., and Cluzel, P. (2012). Mechanism-independent method for predicting response to multidrug combinations in bacteria. Proc. Natl. Acad. Sci. USA *109*, 12254–12259.

Wu, J., Zhang, N., Hayes, A., Panoutsopoulou, K., and Oliver, S.G. (2004). Global analysis of nutrient control of gene expression in Saccharomyces cerevisiae during growth and starvation. Proc. Natl. Acad. Sci. U S A *101*, 3148–3153.

Zimmer, A., Katzir, I., Dekel, E., Mayo, A.E., and Alon, U. (2016). Prediction of multidimensional drug dose responses based on measurements of drug pairs. Proc. Natl. Acad. Sci. USA *113*, 10442–10447.

Zimmer, A., Tendler, A., Katzir, I., Mayo, A., and Alon, U. (2017). Prediction of drug cocktail effects when the number of measurements is limited. PLoS Biol. *15*, e2002518.

Please cite this article in press as: Lukačišin and Bollenbach, Emergent Gene Expression Responses to Drug Combinations Predict Higher-Order Drug Interactions, Cell Systems (2019), https://doi.org/10.1016/j.cels.2019.10.004

STAR★METHODS

KEY RESOURCES TABLE

REAGENT or RESOURCE	SOURCE	IDENTIFIER
Chemicals, Peptides, and Recombinant Proteins		
Lithium chloride	Sigma Aldrich	L9650
Cycloheximide	Sigma Aldrich	37094
Myriocin	Sigma Aldrich	M1177
Rapamycin	Sigma Aldrich	37094
Yeast extract	Sigma Aldrich	Y1625
Peptone	Sigma Aldrich	91249
Dextrose	Sigma Aldrich	D9434
Methyl methanesulfonate	Sigma Aldrich	129925
Glycerol	Sigma Aldrich	G5516
Critical Commercial Assays		
RiboPure RNA Purification Kit for yeast	Thermo Scientific	AM1926
NEBNext Magnesium RNA Fragmentation Module	New England Biolabs	E6150S
Dynabeads oligo-dT kit	Invitrogen	61012
Agencourt AMPure XP	Beckman Coulter	A63881
Quick Ligation Kit	New England Biolabs	M2200S
KAPAHiFi Hot-Start ReadyMix	VWR	733-2430
RNase H	New England Biolabs	M0297S
Deposited Data		
RNA sequencing data	GEO	GSE138256
Experimental Models: Organisms/Strains		
Saccharomyces cerevisiae BY4741	EuroScarf	Y00000
Software and Algorithms		
Matlab	Mathworks	
TopHat	Kim et al., 2013	
UMI-tools	Smith et al., 2017	
featureCounts	Liao et al., 2014	
Gorilla	Eden et al., 2009	

LEAD CONTACT AND MATERIALS AVAILABILITY

Further information and requests for resources should be directed to and will be fulfilled by the Lead Contact, Tobias Bollenbach (t.bollenbach@uni-koeln.de). This study did not generate new unique reagents.

EXPERIMENTAL MODEL AND SUBJECT DETAILS

Saccharomyces cerevisiae strain BY4741 was obtained from EuroScarf repository, cat. No. Y00000.

METHOD DETAILS

Automated Re-inoculation Setup for Reproducible Yeast Culture

Saccharomyces cerevisiae strain BY4741 was grown in 20 ml of YPD broth - yeast extract (Sigma Aldrich cat. No. Y1625), peptone (Sigma Aldrich cat. No. 91249), dextrose (Sigma Aldrich cat. No. D9434) in a 100 ml conical flask shaken 220 rpm at 30°C overnight and then distributed into a 96-well plate (non-treated transparent flat bottom, Nunc). A customized liquid handling robot (Tecan Freedom Evo 150) with 8 liquid handling channels and a robotic manipulator was used to produce a two-dimensional discretised two drug 24 × 24-well gradient in YPD spread over six 96-well plates and to inoculate the yeast overnight culture to final optical

density at 600 nm (OD_{600}) of 0.15 and final liquid volume in the well of 200 μl. The discretized drug gradient was set up as in Chevereau and Bollenbach (2015), that is the concentration of each drug was spaced according to $c = c_{max}(x^3 + ax)/(1 + a)$, where c_{max} was the highest concentration used, x was linearly spaced from 0 to 22 steps (with replicate for no drug condition) and $a = 1/3$. Working drug solutions were prepared either by adding the respective amounts of concentrated DMSO drug stocks thawed from −20°C storage (no refreezing) previously prepared from stock chemicals (cycloheximide cat. No. 37094, myriocin cat. No. M1177, rapamycin cat. No. 37094, all from Sigma Aldrich), or by dissolving directly in YPD and sterile-filtering (LiCl, cat. No. L9650 Sigma Aldrich). The six plates were incubated for three iterations, each lasting ~8 h. Each iteration consisted of incubation and a re-inoculation. Plates were incubated in an automated incubator (Liconic Storex) kept at 30°C, >95% humidity, vigorously shaken at >1,000 rpm. During the incubation, OD_{600} was measured every ~15 min in a Tecan Infinite F500 plate reader. In addition to shaking during incubation, directly before each measurement, plates were shaken on a magnetic shaker (Teleshake; Thermo Scientific) at 1,100 rpm for 20 s. During re-inoculation, a volume V_i of yeast culture specifically calculated for each well so as to achieve OD_{600}=0.15 after dilution (while 1.5 μl $\leq V_i \leq$ 100 μl) was added to a fresh medium in a new 96-well plate containing a drug cocktail pipetted in such a way that the final concentration of both drugs, when accounted for the size of the inoculum, was the same as before the re-inoculation step, and the total volume of liquid in the well was 200 μl. During the re-inoculation the plate to be re-inoculated was not shaken for a max. of 15 mins. The entire setup was kept in a climate room at 30°C and ~50% humidity. The growth rate for each well for each iteration was quantified from the OD_{600} increase over time by a linear fit of $\log_2(OD_{600})$ for the last 10 measurements (~2.5 h) before re-inoculation. All growth rates were normalized to the growth rate of the parent strain in the absence of any drugs measured on the same day.

RNA Extraction and Sequencing

For RNA extraction, wells growing at a relative growth rate close to 50% at the end of the third iteration of the automated re-inoculation culture were selected. RNA extraction was performed using the RiboPure RNA Purification Kit for yeast (Thermo Scientific, cat. No. AM1926). The purity of extracted RNA was confirmed for selected samples using the Agilent RNA 6000 Nano Bioanalyzer Kit. The library was prepared as in (Bar-Ziv et al., 2016). In brief, the purified RNA was fragmented using the NEBNext® Magnesium RNA Fragmentation Module (New England Biolabs cat. No. E6150S), poly(A)-selected using Dynabeads oligo-dT kit (Invitrogen, cat. No. 61012) and reverse-transcribed to cDNA using custom poly(T) primers barcoded for multiplexing as well as containing 4-nt-long unique molecular identifier. The resulting complementary DNA strands were pooled and purified [RNase H (NEB cat. No. M0297S), Agencourt AMPure XP (Beckman Coulter cat. No. A63881)], a custom double-stranded adapter ligated to the 3′ end using Quick Ligation Kit (NEB cat. No. M2200S), second cDNA strand synthesized with KAPAHiFi Hot-Start ReadyMix (VWR cat. No. 733–2430), amplified and 50 bp single-end sequenced on Illumina HiSeq 2500 using a primer complementary to the adaptor at the end opposite to the poly(A).

Diauxic Shift Measurements

S. cerevisiae strain BY4741 was grown in YPD broth overnight and diluted ~100-fold into YPG medium [yeast extract (Sigma Aldrich cat. No. Y1625), peptone (Sigma Aldrich cat. No. 91249), glycerol (Sigma Aldrich cat. No. G5516), final glycerol conc. 3% v/v] containing varying amounts of myriocin or cycloheximide. The antifungal drugs were arranged in an exponential gradient created by 2-fold serial dilution. The cultures were incubated in a 96-well microplate in total volume of 200 μl, in an automated incubator (Liconic Storex) kept at 30°C, > 95% humidity, vigorously shaken at >1,000 rpm; OD_{600} was measured every ~30 min in a Tecan Infinite F500 plate reader. In addition to shaking during incubation, directly before each measurement, plates were shaken on a magnetic shaker (Teleshake; Thermo Scientific) at 1,100 rpm for 20 s.

Three-Drug Interaction Measurements

For three-drug interaction assays, *S. cerevisiae* strain BY4741 was diluted into YPD medium (5×10^3-fold final dilution) from a thawed overnight culture kept at −80°C with 15% glycerol. An 8 × 8 × 8 discretized gradient of the respective drugs was prepared by serial dilution and distributed across eight 96-well plates. The plates were sealed with Parafilm M and shaken at ~1,000 rpm on a Titramax 1000 shaker in a 30°C incubator overnight. The next day, measurements were performed manually approximately every hour in a Biotek Synergy H1 microplate reader. The plates were re-sealed with Parafilm after each measurement, and incubation was continued as before. Growth rates for each well were quantified from the OD_{600} increase over time by a fit to the linear section of $\log_2(OD_{600})$ in the range $0.01 \leq OD_{600} \leq 3$.

QUANTIFICATION AND STATISTICAL ANALYSIS

The reads resulting from sequencing were demultiplexed, aligned to annotated reference *S. cerevisiae* genome R64-2 using TopHat (Kim et al., 2013), deduplicated using UMI-tools (Smith et al., 2017) and quantified using featureCounts (Liao et al., 2014). Gene expression changes were further analyzed using custom written MATLAB scripts. Briefly, to account for sample-to-sample variation and low molecule noise, quantile normalization was applied using the *quantilenorm* function over the entire dataset, and the most highly expressed two-thirds of the genes were used for further analysis. Principal component (PC) analysis was performed for

Please cite this article in press as: Lukačišin and Bollenbach, Emergent Gene Expression Responses to Drug Combinations Predict Higher-Order Drug Interactions, Cell Systems (2019), https://doi.org/10.1016/j.cels.2019.10.004

each drug combination separately using MATLAB function *pca* on $\log_2$ values of gene expression data normalized to the median expression in YPD medium containing no drug, median-filtered along the growth isobole. Results along the growth isobole were visualized using the relative drug fraction $\theta_A = \frac{c_A}{IC_{50}^A} / \left(\frac{c_A}{IC_{50}^A} + \frac{c_B}{IC_{50}^B} \right)$. Gene ontology enrichment analysis for genes up- or down-regulated and strongly governed by the third PC was performed by sorting the genes by their relative third PC loading in descending or ascending order, respectively, and looking for Gene Ontology (GO) terms enriched in the upper part of the list (all possible partitions) using GOrilla (Eden et al., 2009). The relative third PC loading for each gene was calculated by dividing the third PC loading for that gene by the Euclidean norm of the vector containing loadings for all the principal components for that gene. GO terms associated with retrotransposon activity were disregarded in the analysis. Gene enrichment analysis for genes up- or down-regulated and strongly governed by the second PC was performed analogously, except for each drug the relative second PC loadings were averaged across experiments containing the respective drug. Before averaging, the sign of the second PC coefficients and loadings was inverted for experiments where the respective drug is shown on the left side of the x-axis in Figure 3A, so as to ensure consistency in keeping the relative second PC positive if the gene was upregulated in that drug.

DATA AND CODE AVAILABILITY

The RNA sequencing dataset generated during this study is available at the Gene Expression Omnibus, accession code GSE138256.